QED with a spherical mirror

G. Hétet,[1,2] L. Slodička,[1] A. Glätzle,[3] M. Hennrich,[1] and R. Blatt[1,2]
[1]*Institute for Experimental Physics, University of Innsbruck, Technikerstrasse 25, A-6020 Innsbruck, Austria*
[2]*Institute for Quantum-Optics and Quantum Information, Austrian Academy of Science, Otto-Hittmair-Platz 1, A-6020 Innsbruck, Austria*
[3]*Institute for Theoretical Physics, University of Innsbruck, Technikerstrasse 25, A-6020 Innsbruck, Austria*
(Received 13 September 2010; published 9 December 2010)

We investigate the quantum electrodynamic (QED) properties of an atomic electron close to the focus of a spherical mirror. We first show that the spontaneous emission and excited-state level shift of the atom can be fully suppressed with mirror-atom distances of many wavelengths. A three-dimensional theory predicts that the spectral density of vacuum fluctuations can indeed vanish within a volume λ^3 around the atom, with the use of a far-distant mirror covering only half of the atomic emission solid angle. The modification of these QED atomic properties is also computed as a function of the mirror size, and large effects are found for only moderate numerical apertures. We also evaluate the long-distance ground-state energy shift (Casimir-Polder shift) and find that it scales as $(\lambda/R)^2$ at the focus of a hemispherical mirror of radius R, as opposed to the well-known $(\lambda/R)^4$ scaling law for an atom at a distance R from an infinite plane mirror. Our results are relevant for investigations of QED effects as well as free-space coupling to single atoms using high-numerical-aperture lenses.

DOI: 10.1103/PhysRevA.82.063812 PACS number(s): 12.20.−m, 42.25.−p, 37.30.+i

I. INTRODUCTION

Spontaneous emission and level shifts of atoms can be notably altered by placing them between mirrors. By modifying the electromagnetic mode structure interacting with the atomic electron [1], one obtains a significant change in these quantum electrodynamic (QED) atomic properties. Most experimental studies make use of high-finesse cavities [2–7] to see the effects. Another way to change the properties of single emitters is to place other identical atoms nearby, as originally propounded by Dicke [8]. To observe large QED effects in this case, the dipole emission patterns have to overlap, which requires the atoms to be very close to each other. Such effects were analyzed using two trapped ions [9], but the Coulomb interaction between the ions restricted their distance to a few micrometers. The interaction between two neutral atoms is not overwhelmed, however, by the Coulomb force. Using the large dipole moments of nearby Rydberg atoms localized in a dipole trap, entanglement between neutral atoms was recently demonstrated [10,11].

In general, an atom close to a single mirror already provides a very efficient way to investigate QED effects. The resonance fluorescence of a Doppler-cooled barium ion is reflected back onto itself in Ref. [12], using a large-numerical-aperture (NA) lens and a mirror that was 30 cm away from the ion. In this experiment, the description of the interaction between the atom and the modified electromagnetic field, or the mirror image, is very similar to the direct dipole-dipole coupling between two real atoms. Here, because of the high numerical aperture of the collection lens, the mode structure was altered significantly even if the mirror was many wavelengths away from the ion. A 1% change in the decay rate was measured and found to be mostly limited by the collection solid angle and residual atomic motion. Such a system also leads to a vacuum-induced level shift in a laser-excited atom. This has been measured in Ref. [13] and found to be in good agreement with theoretical work [14].

A closely related field of research investigates the absorption of photons from single atoms in free space. Theory predicts that the best possible absorption between an incoming field and a single atom arises when the incoming field matches the spatial atomic radiation mode [15,16]. Recent experiments have demonstrated substantial extinctions from single molecules [17–19], atoms [20,21], and quantum dots [22] in free space, thus showing the potential of free-space coupling with high-NA optics for fundamental investigation of light-matter interactions.

The aforementioned studies make use of the interaction of a real photon with single atoms. The number of experiments investigating Casimir forces between dielectric materials, which are the result of the modification of the mode density of virtual photons, has also rapidly increased. Such studies are now being undertaken with an unprecedented level of precision (see, for example, Ref. [23] and references therein). The comparison with the theory in this field is now reaching good agreement for some geometries and over a wide range of materials. The possibility of using these measurements to gain a better control over nano-mechanical systems and for precise tests of QED has been a major force driving this research. Although many geometries have been investigated theoretically over the past few decades [24], there are still many ongoing investigations into the sign of the force [25], or the accuracy of the proximity force approximations [26], for estimating Casimir shifts of various materials.

For atoms close to dielectrics, the modification of the ground-state level shift (Lamb shift) yields the well-known Casimir-Polder force [27], which is observed in Ref. [7] for a plane mirror geometry. The Casimir-Polder force was not reported or calculated for single well-localized atoms around complex opened three-dimensional (3D) geometries. It is expected that such investigations would also provide efficient ways to test the behavior of vacuum fluctuations.

Here we demonstrate that a spherical mirror covering half of an atomic dipole emission profile can fully suppress its spontaneous emission and excited-state level shifts provided that the mirror is close enough to allow temporal interference of the field amplitudes (Markov limit). We also calculate the shift of the ground state, the Lamb shift, as a function of mirror

distance and find a scaling law that is more favorable than the plane mirror geometry for observing large shifts. Because of the development in the control of atomic motion [28] and mirror and lens fabrication [29], these effects are now within experimental reach.

The modification of spontaneous emission and level shifts is first calculated using a one-dimensional model where the electron radiates along the mirror axis. We find full suppression of the vacuum fluctuations coupling to the atomic electron, even with a single mirror. The physical origin of this complete cancellation lies in the high spatial and temporal interference between the plane-wave modes going to the mirror and the modes going to free space so that the density of vacuum fluctuations can reach zero around this idealized atom. Similar calculations were performed by several authors to model more realistic scenarios (see, for example, Refs. [14,30] and references therein) with the inclusion of free-space vacuum modes that do not interfere with the mirror modes; therefore full extinction of spontaneous emission was not explicitly considered. We furthermore extend the one-dimensional (1D) calculations to a 3D theory that goes beyond the paraxial approximation and demonstrate that the effective coupling to vacuum modes around an atomic electron can also reach zero within a volume λ^3 around the focus of a spherical mirror. We show that, in the spherical basis, the effect can be understood as the result of an ideal interference between all the even modes. Last, the long-distance ground-state energy shift (Casimir-Polder shift) is evaluated using the complete set of normal modes of the spherical mirror. We find that the Casimir-Polder shift scales as $(\lambda/R)^2$ for a half mirror of radius R and atomic transition wavelength λ, as opposed to the well-known $(\lambda/R)^4$ scaling law for a plane mirror, where R is the mirror distance from the atom.

A wealth of studies exists on this topic. We would like to point out that, to the best of our knowledge, theoretical efforts have concentrated on plane geometries [30–33], cavities in the paraxial approximation [1,3], dielectric spheres [34–38], or parabolic mirrors [39]. Closely related work was done, however, for a large spherical open cavity by Daul and Grangier [40]. Strong enhancement and inhibition of vacuum fluctuations were found with moderate cavity finesses, and a full set of normal modes was derived for the symmetric geometry. The case of a single mirror was found by setting the second mirror reflectivity to zero in a more general formula for the density of vacuum fluctuations in an asymmetric cavity. In Sec. IV, we present a different route toward finding the normal mode amplitudes in the single-mirror geometry, which we use further for the Casimir-Polder shift calculation.

We would like to stress that all the calculations are performed in the limit where the mirror is many wavelengths away from the atom ($k_0 R \gg 1$). This simplifies the theoretical treatments and experimental approach greatly, yet allows strong QED effects to be observed. Let us also mention here that, since we use a single mirror, the QED effects for an exited atom are easier to understand here as a modulation of the electron coupling to certain modes rather than as a change in the mode density [3].

II. ATOMIC DECAY AND LEVEL SHIFTS

It is well known that coupling an initially excited atom to a reservoir of electromagnetic field modes in the vacuum state yields a spontaneous decay to the ground state and shifts its excited-state energy. Also, when the atom is in the ground state, its energy is shifted because of absorption and reemission of virtual photons, the so-called Lamb shift. When the electromagnetic field modes are modified by nearby dielectric boundaries, these QED properties therefore are changed. Another picture, using radiation self-reaction only, can also be employed to describe the modification of QED properties [30]. To find the relative contribution of both vacuum and self-reaction mechanisms, the dynamics of the corresponding quantities in the differential equation one wishes to interpret has to be Hermitian [41,42]. When this is done, both effects are found to contribute to the same degree.

The free part of the light-atom Hamiltonian is the sum of the atomic and optical rest energies,

$$\hat{H}_0 = \frac{1}{2}\hbar\omega_0\hat{\sigma}_z + \sum_\mu \hbar\omega_\mu \left(\hat{a}_\mu^\dagger \hat{a}_\mu + \frac{1}{2}\right), \tag{1}$$

where $\hat{\sigma}_z = \hat{\sigma}_{11} - \hat{\sigma}_{22}$ is the population difference between the upper and lower atomic states, and $\hat{a}_\mu$ is the creation operator for a photon in a mode μ of the reservoir. Here ω_0 is the atomic transition frequency, and ω_μ is the frequency of the optical mode μ. The frequency of the optical modes is quantized using the boundary condition on a large cavity. In spherical coordinates we use a large quantization sphere of radius Λ, as depicted in Fig. 1.

The interaction Hamiltonian in the Coulomb gauge and in the electric dipole approximation is

$$\hat{H}_{\text{int}} = -\frac{e}{mc}\hat{A}(\vec{r},t)\cdot\hat{p} + \frac{e^2}{2mc^2}\hat{A}^2(\vec{r},t), \tag{2}$$

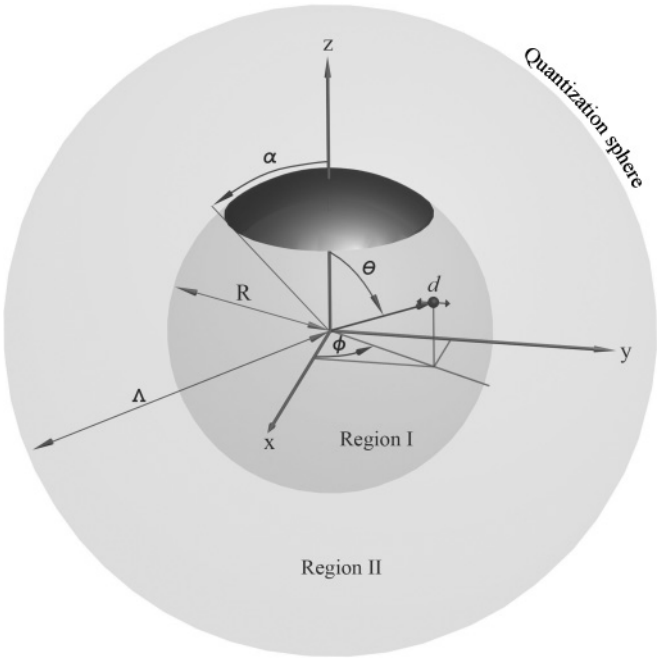

FIG. 1. Schematics of the mirror and notation used to calculate the QED properties for an atomic dipole $\vec{d}$ in region I. The mirror has an aperture α and a radius of curvature R.

where $\hat{p}$ is the momentum of the atomic electron, $\vec{r}$ its position (i.e., the position of the atomic nucleus in the electric dipole approximation), and m its mass. Here $\hat{p}$ will be written in terms of the electric dipole matrix element $\vec{d}$ of the two-level atom as $m\omega_0\vec{d}/e \times \hat{\sigma}_y$, where $\hat{\sigma}_y := i(\hat{\sigma}_{12} - \hat{\sigma}_{21})$, and $\hat{A}$ is the potential vector. We decompose it over a complete mode basis $\vec{e}_\mu$ as

$$\hat{A}(\vec{r},t) = \sum_\mu \sqrt{\frac{2\pi\hbar c^2}{\omega_\mu}}\vec{e}_\mu(\vec{r})\hat{a}_\mu(t) + \text{H.c.}, \tag{3}$$

where the sum is to be taken over *all normalized* eigenfunctions $\vec{e}_\mu$ of the Helmholtz equation.

In the Markov regime, which is when the reservoir and atom are correlated only within a short time, one *can define* the spontaneous emission rate and level shifts and, after solving the Heisenberg equation, get

$$\frac{\partial}{\partial t}\langle\hat{\sigma}(t)\rangle = -\{\gamma(\vec{r})/2 + i[\Delta_e(\vec{r}) - \Delta_g(\vec{r})]\}\langle\hat{\sigma}(t)\rangle,$$

where $\langle\cdot\rangle$ denotes the expectation value over a separable atom-vacuum product state. We write

$$\gamma(\vec{r}) = 2\sum_\mu |g_\mu(\vec{r})|^2\delta(\omega_\mu - \omega_0), \tag{4}$$

$$\Delta_{g,e}(\vec{r}) = \sum_\mu |g_\mu(\vec{r})|^2 \mathrm{P}\left(\frac{1}{\omega_\mu \pm \omega_0}\right), \tag{5}$$

where $\pm$ holds for the ground- (excited-) state shifts, respectively P denotes the principal part, and

$$g_\mu(\vec{r}) = \omega_0\sqrt{\frac{2\pi}{\hbar\omega_\mu}}[\vec{d}\cdot\vec{e}_\mu(\vec{r})] \tag{6}$$

is the vacuum Rabi frequency of the mode μ. The sum over the μ eigenmodes runs up to the Bethe momentum cutoff, $K = mc/\hbar$ [30].

The excited-state level shift Δ_e is due to the emission of real photons, whereas the ground-state level shift arises from absorption and emission of virtual photons from the vacuum reservoir [30]. To obtain the correct Lamb shift in the nonrelativistic theory, however, we have to add the term proportional to $\hat{A}^2$ in the interaction Hamiltonian, which was actually discarded when obtaining Eq. (5). We return to this in Sec. V B, where we calculate the Lamb shift in the 3D case.

We would like to emphasize that as we consider the atom only to be far from the mirror ($k_0R \gg 1$, where $k_0 = \omega_0/c$), the modification of the vacuum *mode density* affects the atom only if it is in the ground state [43]. The change in the excited-state properties here are due to a pure self-*interference* of the electromagnetic modes to which the excited atom can couple [30,43]. We will then neglect the dependence of the coupling strength on ω_k for the excited level shift, which comes down to ignoring energy level shifts (van der Waals shifts) that are significant only if the mirror is very close to the atom. For a two-level atom, these shifts are identical for the excited and ground states [43], so the total "near-field" energy shift would remain unaffected by the presence of the mirror anyway.

Before moving to the three-dimensional results, and to gain physical insight into the process of emission and energy shifts in the presence of a mirror, we first perform a one-dimensional calculation.

III. ONE-DIMENSIONAL MODEL

In this section, we assume that the atom can couple to the electromagnetic fields only through a set of one-dimensional spatial modes k along the mirror axis z. This means that the other modes do not contribute to spontaneous emission. This situation, of course, bears a similarity to the spherical mirror case, where half of the light field is also reflected back to the atom, and is therefore worth investigating in some detail.

A. Normal mode and quantization

The scalar, one-dimensional mode functions $e_k(z)$ of the problem must satisfy the Helmholtz equation

$$\nabla^2 e_k(z) + |k|^2 e_k(z) = 0. \tag{7}$$

The solutions are superpositions of plane waves traveling in reverse directions. We assume that the (one-dimensional) quantization domain has a length L, the atom is at $z = 0$, and the mirror is at $z = -R$. The density of k modes is readily found to be $L/2\pi$ from the periodic boundary conditions at $z = L$. From the boundary condition on the mirror $e_k(z = -R) = 0$, and after normalizing each mode to unity, we find that the mode functions can be written as

$$e_k(z) = \frac{1}{\sqrt{2L\mathcal{A}}}(e^{ikz} - e^{-2ikR}e^{-ikz}), \tag{8}$$

where $\mathcal{A}$ is the transverse cross-sectional area of the field around the atom. It is clear from this relation that the wave going to the mirror (second term) and the wave going directly to free space (first term) will interfere perfectly provided temporal coherence is fulfilled.

Using this mode function, we now compute the influence of the mirror on an excited atom, i.e., on *real photon* processes.

B. Real photon processes and an atom in the excited state

We neglect here the modification of the mode spectral density that couples to the excited atom and consider the modification of the atomic state due to self-interference, as already discussed, so we neglect the dependence of g_μ on ω_μ. In the Markov regime, using Eqs. (4) and (5), we find that the atomic coherence decay and excited-state level shift at $z = 0$ are then [14]

$$\gamma(0) = \gamma_{\mathrm{FS}}[1 - \cos(2k_0R)], \tag{9}$$

$$\Delta_e(0) = \gamma_{\mathrm{FS}}\sin(2k_0R), \tag{10}$$

where the free-space 1D spontaneous emission rate is

$$\gamma_{\mathrm{FS}} = \frac{2d^2\omega_0}{\hbar\mathcal{A}}. \tag{11}$$

For $2k_0R = 2\pi n$ (where n is an integer number), we get a complete suppression of spontaneous emission and excited level shift. On the other hand, for $2k_0R = \pi n$, the spontaneous emission is enhanced by a factor of 2.

The reason for such large effects is that the fields going to the mirror and the "direct" fields can fully interfere in the Markov regime. To find out in which regime temporal coherence is not satisfied, so that the visibility of the single-photon interference is not perfect, we would need to consider the exact quantum dynamical evolution without making a Markov

approximation. Such an analysis would reveal that temporal coherence is reduced when the mirror is placed such that the time it takes for the light field to go to the mirror and back is longer than the atom decay time. This scenario is investigated, for example, in Ref. [14] and studied experimentally in Ref. [44], where signatures of non-Markovian dynamics were analyzed using a Hanbury-Brown and Twiss setup. It was noted that bunching appears for short time scales, similar to the bunching that would appear for two classical sources (which here would be the atom and its far-distant mirror image).

In the "extreme" non-Markovian regime, where the mirror is placed far away from the atom, a multimode field with width $1/\gamma_{\rm FS}$ is emitted toward the mirror with 50% probability. The other half goes to free space. The atom is completely in the ground state when this field returns from the mirror. It will reexcite the atom after a time $\tau = 2R/c$, but only partially since its temporal envelope is not the time-reversed spontaneously emitted field [16] and its amplitude is half as large. After such a (partial) reexcitation, another field will be emitted along the mirror so that the atom will again be reexited later. Eventually, the photon will leave after a complex dynamical process that resembles that of a multimode cavity [14,45]. In this paper, we always assume Markovian dynamics, where a linear decay and level shifts can be defined. We will be concerned only with spatial decoherence, by assuming ideal temporal overlap of the single photon with itself, i.e., $\tau \ll 1/\gamma_{\rm FS}$.

We have assumed here that the atom couples only to the longitudinal modes along the mirror axis, which is not realistic for an atom in free space. We will now calculate the effects of polarization and use a spherical mirror, and we will show that similar behavior appears for a full hemisphere; that is, in the Markovian regime, spontaneous emission and excited-state level shifts can be suppressed. We also calculate the far-field Casimir-Polder shift and compare it with the well-known calculations of the Casimir-Polder shift for an atom close to an infinite plane mirror.

IV. THREE-DIMENSIONAL MODEL

In this section, the space will be divided into a part inside a sphere of radius R (region I) and the annular region between the sphere of radius R and the quantization sphere (region II). See Fig. 1.

A. Normal modes

In spherical coordinates, $\mu = (l,m,\sigma)$, where σ denotes the transverse electric (TE) or transverse magnetic (TM) modes, and (l,m) are the quantum numbers for the angular momentum and spin, respectively. The solution of the Maxwell equation for the electric field can be written as a superposition of the electric and magnetic multipoles [46]:

$$\vec{e}_{\rm TM}(\vec{r}) = g_l(k_\mu r)\vec{X}_{l,m}(\vec{\Omega}), \tag{12}$$

$$\vec{e}_{\rm TE}(\vec{r}) = \frac{i}{k_\mu}\vec{\nabla} \times [f_l(k_\mu r)\vec{X}_{l,m}(\vec{\Omega})], \tag{13}$$

where $\vec{X}_{l,m}(\vec{\Omega}) = \vec{L}Y_{l,m}(\vec{\Omega})/\sqrt{(l+1)}$ is the vectorial spherical harmonic, f_l, g_l are superpositions of spherical Bessel or Hankel functions, $\vec{\Omega}$ is the vectorial solid angle along the radial direction $\vec{r}$, and $\vec{L} = \vec{r} \times \vec{p}$ is the angular momentum operator. The magnetic induction $\vec{B}$ is a superposition of the two multipoles:

$$\vec{b}_{\rm TM}(\vec{r}) = \frac{-i}{k_\mu}\vec{\nabla} \times [g_l(k_\mu r)\vec{X}_{l,m}(\vec{\Omega})], \tag{14}$$

$$\vec{b}_{\rm TE}(\vec{r}) = f_l(k_\mu r)\vec{X}_{l,m}(\vec{\Omega}). \tag{15}$$

The radial functions are written as

$$\begin{aligned} g_l(k_\mu r) &= c_l j_l(k_\mu r) \quad \text{in region I,} \\ &= a_l h_l^{(1)}(k_\mu r) + b_l j_l(k_\mu r) \quad \text{in region II,} \end{aligned} \tag{16}$$

where $h_l^{(1)}(k_\mu r)$ is the spherical Hankel function and $j_l(k_\mu r)$ is the spherical Bessel function of the first kind. It is clear that, in the absence of the mirror, the b_l modes are the vacuum field from region II. We will show next that, in the single-mirror geometry, we need only to quantize these modes.

B. Quantization

We will not solve the full quantum mechanical problem by quantizing the electromagnetic field in the presence of the spherical mirror. This can be done exactly in the case of a full sphere [35] by solving the eigenvalue equation derived from the boundary conditions. To the best of our knowledge, such a treatment has not been done for an open geometry such as a hemispherical mirror. As is shown in Ref. [40], the problem is not so difficult, however, if one assumes that the boundary condition lies in the far field ($k_0 R \gg 1$), as we assume here, so that the mode density is close to that of free space. We are then mostly dealing with a continuum of modes, such as in the 1D calculations.

Using the boundary condition on the large quantization sphere, we find that

$$k_l \Lambda = l\frac{\pi}{2}. \tag{17}$$

The density of free-space vacuum modes is then $2\Lambda/\pi$. From a point close to the focal point, the b_l modes are nondegenerate if the mirror is large enough, so they are all orthogonal to each other. We normalize them so that each contains one photon. For the magnetic multipole we then require that

$$\int_0^\Lambda r^2 dr |g_l(kr)|^2 \int_{4\pi} d\vec{\Omega} |\vec{X}_{l,m}(\Omega)|^2 = 1. \tag{18}$$

In free space, $a_l = 0$, and we thus get the condition

$$|b_l|^2 \approx \frac{k^2}{2\Lambda}, \tag{19}$$

where we use the fact that the main contribution to the vacuum fluctuations stems from the far field. The same relation holds for the vacuum modes of the electric multipole.

C. Free-space decay

Having normalized the vacuum modes b_l, and the normal modes of the system, we can calculate the distribution of vacuum fluctuations and atomic properties in region I and associate the eigenmodes b_l to the continuous set $\vec{k}$, so that $\sum_\mu \to (\Lambda/\pi)\int dk \sum_{l,m}$. For a dipole oriented along $\vec{r}$, for example, we can check that we get the usual free-space

spontaneous decay. Using Eq. (4), the formula for the field component along the radial direction (see the Appendix), and setting a_l to zero in Eq. (16), we indeed find that

$$\gamma_{\rm FS} = \frac{\Lambda}{\pi}\int dk \sum_{l,m} |b_l|^2 l(l+1)\frac{j_l^2(kr)}{(kr)^2}|Y_{l,m}|^2 \times \frac{2\pi\omega_0^2 d^2}{\hbar\omega_k}\delta(\omega_k-\omega_0) \tag{20}$$

$$= \frac{d^2\omega_0^3}{3\pi\hbar c^3}, \tag{21}$$

which is the standard spontaneous decay rate of an atom in free space. In the last step, we used the addition formula for spherical harmonics $\sum_m |Y_{l,m}|^2 = (2l+1)/4\pi$ and the addition formula

$$\sum_{l=1} l(l+1)(2l+1)\frac{j_l^2(kr)}{(kr)^2} = \frac{2}{3}. \tag{22}$$

One can show that the spontaneous decay rate is the same for a tangential dipole orientation.

In the following discussion, we will see how the mirror imposes a fixed phase relation between the even and odd l modes appearing in Eq. (22) used in the spontaneous decay calculation and how this modifies it. This can be seen by noting that

$$\sum_{l \text{ even or odd}} l(l+1)(2l+1)\frac{j_l^2(kr)}{(kr)^2} = \frac{2}{3}\int_0^{\pi/2} d\theta \sin^3\theta \begin{bmatrix}\sin^2(kr\cos\theta)\\ \cos^2(kr\cos\theta)\end{bmatrix}, \tag{23}$$

where the odd (even) modes correspond to the sine (cosine) functions. Depending on whether the atom is at the node or the antinode of the standing wave, it couples preferentially to the even or odd modes. Without a defined phase relation between even and odd l modes, as is the case for free space, their spectral densities always add up to $2/3$ as we just saw, but they can otherwise cancel or add up coherently. This will allow suppression or enhancement of the even or odd vacuum mode fluctuations and thus create significant changes in the decay and shifts.

D. Boundary conditions

The boundary conditions on the electric and magnetic fields are

$$\vec{n}\times\vec{E}^{\rm I}|_{r=R} = \vec{n}\times\vec{E}^{\rm II}|_{r=R}, \tag{24}$$

$$\vec{n}\times\vec{B}^{\rm I}|_{r=R} = \vec{n}\times\vec{B}^{\rm II}|_{r=R}, \tag{25}$$

for $\theta\in[\alpha,\pi]$ and $\phi\in[0,2\pi[$ (see Fig. 1), where $\vec{n}$ is the normal to the mirror. We write $\vec{E}^{\rm I,II}$, the electric field in regions I and II. Assuming that the mirror is a perfect conductor, as we always do in this paper, we also have

$$\vec{n}\times\vec{E}^{\rm I}|_{r=R} = \vec{0}, \tag{26}$$

$$\vec{n}\cdot\vec{B}^{\rm I}|_{r=R} = 0, \tag{27}$$

for $\theta\in[0,\alpha[$ and $\phi\in[0,2\pi[$.

Two sets of equations for the transverse electric and magnetic multipoles can then be obtained and solved for c_l to calculate the total field in region I.

E. System of equations

We use the symmetry along ϕ by projecting the boundary conditions over the m modes (multiplication by $e^{im\phi}$ and integration over ϕ). From Eq. (26) we get, for example, for the θ component of the TM mode, the relation

$$\sum_{l=1}^{\infty} g_l^{\rm I}(kR)A_{l,m}(\theta) = 0 \quad \text{for } \theta\in[0,\alpha[, \tag{28}$$

where

$$A_{l,m}(\theta) = \sqrt{\frac{(2l+1)(l-m)!}{(l+m)!}}\frac{P_l^m(\cos\theta)}{\sqrt{l(l+1)}} \tag{29}$$

and P_l^m is the associated Legendre polynomial. After projecting over m and l, and using the orthogonality of the spherical modes, we require

$$c_l j_l(kR) = a_l h_l^{(1)}(kR) + b_l j_l(kR). \tag{30}$$

Last, we use Eq. (25) and obtain

$$\sum_{l=1}^{\infty}\frac{\partial[rg_l^{\rm I}(kr)]}{\partial r}A_{l,m}(\theta) = \sum_{l=1}^{\infty}\frac{\partial[rg_l^{\rm II}(kr)]}{\partial r}A_{l,m}(\theta) \tag{31}$$

for $\theta\in[\alpha,\pi]$ and $r=R$. Using the Wronskian for spherical Bessel functions, we then get two sets of equations:

$$\sum_{l=1}^{\infty}(c_l-b_l)\frac{A_{l,m}}{h_l^{(1)}(kR)} = 0, \quad \theta\in[0,\alpha[, \tag{32}$$

$$\sum_{l=1}^{\infty} c_l j_l(kR)A_{l,m} = 0, \quad \theta\in[\alpha,\pi], \tag{33}$$

for the coefficients of the magnetic multipole. Similarly, we get

$$\sum_{l=1}^{\infty}(d_l-e_l)\frac{A'_{l,m}}{\left[rh_l^{(1)}(kr)\right]'} = 0, \quad \theta\in[0,\alpha[, \tag{34}$$

$$\sum_{l=1}^{\infty} d_l[rj_l(kr)]'A'_{l,m} = 0, \quad \theta\in[\alpha,\pi], \tag{35}$$

for the electric multipole, where $[rj_l(kr)]' = \partial[rj_l(kr)]/\partial r|r=R$, and $A'_{l,m} = \partial A_{l,m}/\partial\theta$. Here e_l and d_l are the amplitude coefficients for $f_l(kr)$, equivalent to c_l and b_l for $g_l(kr)$. Each set of equations can be written as a Fredholm equation that can be solved numerically [47].

Here we will show that an analytical solution can be found in the limit where $k_0R \gg l(l+1)$, i.e., using a large mirror and/or looking at the field fluctuations close to the focus. We note that the field is orthogonal to $\vec{n}$ far from the origin [see Eq. (A1)]. The condition (27) is then satisfied automatically. In this case, the solutions of the two sets of equations will be identical for both the TE and TM modes, so that the reflection off the mirror will preserve polarization.

The solution can then be found using scalar fields. We will include the polarization dependence of the dipole emission

later, after having identified far-field plane-wave modes. We will write

$$\phi_b(\vec{r}) = \sum_{l,m} c_l\, j_l(kr) Y_{l,m} \tag{36}$$

for the total field amplitude in region I and solve for c_l as a function of b_l using two equations:

$$\sum_{l=0}^{\infty} (c_l - b_l) \frac{Y_{l,m}}{h_l^{(1)}(kR)} = 0, \quad \theta \in [0,\alpha[, \tag{37}$$

$$\sum_{l=0}^{\infty} c_l\, j_l(kR) Y_{l,m} = 0, \quad \theta \in [\alpha,\pi]. \tag{38}$$

We simply removed the $l(l+1)$ dependence of the field modes, which, as can be found from Eq. (23), is equivalent to ignoring the polarization dependence of the dipole emission ($\sin^2\theta$ in the integral). Note that the summation now starts at $l = 0$, as is allowed for scalar fields. This is not true for the general solution of the (vectorial) Maxwell equation, which does not have spherically symmetric solutions.

F. Full-hemispherical mirror

We first assume that the mirror covers 2π sr, so $\alpha = \pi/2$. Furthermore, since $k_0 R \gg l(l+1)$, we expand the Bessel functions in the far field:

$$h_l^{(1)}(kR) \approx (-i)^{l+1} e^{ikR}/kR, \tag{39}$$

$$j_l(kR) \approx \sin(kR - l\pi/2)/kR. \tag{40}$$

Using the relation

$$\int_0^1 P_l^m(x) P_{l'}^m(x)[1 + (-1)^{l+l'}] = 2\frac{\delta_{l,l'}}{2l+1}\frac{(l+m)!}{(l-m)!} \tag{41}$$

in Eqs. (37) and (38) and then solving for c_l, we obtain after some algebra the two relations

$$\begin{aligned} c_{l'} &= e^{ikR}\cos(kR)\left(b_{l'} - i\sum_{m,o} b_l I_{l',l,m}\right) \quad \text{for } l' \text{ even}, \\ c_{l'} &= i e^{ikR}\sin(kR)\left(b_{l'} + i\sum_{m,e} b_l I_{l',l,m}\right) \quad \text{for } l' \text{ odd}, \end{aligned} \tag{42}$$

where

$$I_{l',l,m} = (-1)^{(l+l'+1)/2} \int_\phi \int_{\theta=[0,\pi/2]} Y_{l,m} Y_{l',m} d\vec{\Omega}. \tag{43}$$

We denote $\sum_{o,e}$ as the sum over odd (even) l modes. The two terms on the right-hand side of each equation are the reflected and incoming vacuum amplitude contributions to the field in region I.

At the focus, only the $l' = 0$ mode is predominant since the radial amplitudes [given by $j_{l'}(kr)$] are negligible for higher l'. The total field $\phi_b(\vec{r})$ at the center will then be zero for $kR = n\pi$, as can be seen from Eqs. (42) and (36). If we draw any standing wave from the mirror through the origin to the other free-space boundary with the condition that $kR = n\pi$, it is then invariant under rotation upon θ. It follows that to completely describe the field in region I when the total field is zero at the focus, we need only even modes [as is apparent from Eq. (42)]. For the case where $kR = n\pi/2$, however, we will need the odd modes to find the total field in region I. These two extremal conditions explain why even and odd l' modes behave differently with respect to mirror positions, as we already anticipated in Sec. IV C.

We also note that, contrary to what one would find for a mirror covering 4π (which would behave as a cavity), the angular asymmetry of the hemisphere does not yield a one-to-one mapping of the free-space modes $b_{l'}$ of region II to the $c_{l'}$ modes of region I. The total far-field amplitude that can enter region I here is necessarily a superposition of even and odd modes.

We have already showed that the total field at the focal point $\phi_b(\vec{r} = \vec{0})$ will be zero at a node. Spontaneous emission and level shifts will then certainly cancel. To demonstrate this result, and treat the case of a finite mirror size, it is useful to introduce relations between the plane waves and spherical harmonics.

G. Plane-wave decomposition

Let us first write the far-field amplitude in region I as

$$\sum_{l,m} b_l\, j_l(kr) Y_{l,m} = i f^o(\vec{\Omega})\frac{\cos(kr)}{kr} + f^e(\vec{\Omega})\frac{\sin(kr)}{kr}, \tag{44}$$

where

$$f^{e \text{ or } o}(\vec{\Omega}) := \sum_{m,e \text{ or } o} b_l i^l Y_{l,m}(\vec{\Omega}) \tag{45}$$

is the scattering amplitude for the even or odd mode. It is easy to show that the superpositions

$$f^{\text{in}}(\vec{\Omega}) = \frac{i}{2}(f^o - f^e), \quad f^{\text{out}}(\vec{\Omega}) = \frac{i}{2}(f^o + f^e) \tag{46}$$

correspond to incoming and outgoing angular amplitudes, respectively, and that they are connected via

$$f^{\text{out}}(\vec{\Omega}) = -f^{\text{in}}(-\vec{\Omega}) := \hat{P} f^{\text{in}}, \tag{47}$$

where $\hat{P}$ is the parity operator. This relation shows the Gouy phase shift acquired by the incoming field as it turns after focusing into an outgoing field. The same relations also hold for the far-field amplitude $g(\vec{\Omega})$ of the field in region I, where one can define

$$g^{e \text{ or } o}(\vec{\Omega}) := \sum_{m,e \text{ or } o} c_l i^l Y_{l,m}(\vec{\Omega}). \tag{48}$$

The total field amplitude at any point of region I can in fact be written as a superposition of plane waves weighted by the far-field amplitudes $g(\vec{\Omega})$. Using the expansion of the plane waves in spherical harmonics,

$$\sum_{m,e \text{ or } o} i^l (2l+1) j_l(kr) Y_{l,m} = \begin{bmatrix} \cos(\vec{k}\cdot\vec{r}) \\ \sin(\vec{k}\cdot\vec{r}) \end{bmatrix}, \tag{49}$$

and Eqs. (48) and (36), we obtain

$$\phi_b(\vec{r}) = \frac{1}{2\pi}\int_{2\pi} d\vec{\Omega}[g^e \cos(\vec{k}\cdot\vec{r}) + i g^o \sin(\vec{k}\cdot\vec{r})], \tag{50}$$

where we write $\int_{2\pi} := \int_\phi \int_{\theta=[0,\pi/2]}$ for simplicity. The field inside region I is uniquely given by the coefficients $g^{e \text{ or } o}$,

which are linked to the incoming vacuum modes f^{in} via the boundary conditions. This treatment is also used in Ref. [40] for an open cavity.

H. Finite-size mirror

To treat the case of finite mirror size, we decompose the boundary conditions into three interfaces: the mirror ($\theta \in [0,\alpha[$), the opposite free-space interface between regions I and II ($\theta \in [\pi-\alpha,\pi]$), and the remaining free space ($\theta \in [\alpha,\pi-\alpha[$). As before, we project Eqs. (37) and (38) over the m modes and using the results of Sec. IV G obtain the results

$$\begin{aligned}[1-e^{2ikR}T(\theta)]g^{o} &= -2e^{ikR}\sin(kR)[f^{\text{in}}+T(\theta)f^{\text{out}}],\\ [1+e^{2ikR}T(\theta)]g^{e} &= -2ie^{ikR}\cos(kR)[f^{\text{in}}-T(\theta)f^{\text{out}}],\end{aligned} \tag{51}$$

where $T(\theta)$ is a function that is zero for $\theta \in [0,\alpha[$ and unity for $\theta \in [\alpha,\pi/2[$. One can check that by setting $T(\theta)$ to zero for $\theta \in [0,\pi/2[$, and going back to the spherical basis, we find again Eq. (42).

Using Eq. (47), and the fact that T is only zero or one, we can rewrite Eq. (51) as

$$\begin{aligned}g^{o} &= i\{T(\theta)(1-\hat{P})+2i[1-T(\theta)]e^{ikR}\sin(kR)\}f^{\text{in}},\\ g^{e} &= i\{T(\theta)(1+\hat{P})-2[1-T(\theta)]e^{ikR}\cos(kR)\}f^{\text{in}},\end{aligned} \tag{52}$$

which uniquely relates the incoming field from region II to the far-field modes in region I. With the use of the relation (50), we finally obtain the result

$$\phi_b(\vec{r}) = \sum_{l,m} b_l i^l T_{l,m}, \tag{53}$$

where

$$\begin{aligned}T_{l,m} = 2i\int_{2\pi}\frac{d\vec{\Omega}}{4\pi}\{&T(\theta)(e^{i\vec{k}\cdot\vec{r}}+e^{-i\vec{k}\cdot\vec{r}}\hat{P})\\ &+2[1-T(\theta)]e^{ikR}\cos(kR+\vec{k}\cdot\vec{r})\}Y_{l,m}.\end{aligned} \tag{54}$$

The total field in region I is a superposition of waves that travel through the point of coordinate $\vec{r}$ without being reflected by the mirror [first term in Eq. (54)] and waves that are reflected by the mirror (second term), as one can easily figure out. A similar result is found for an open cavity with variable reflectivity in Ref. [40], where the density of modes of a single mirror is calculated by setting one of the mirror reflectivities to zero. Here we derived the normal-mode amplitudes for the case of a single mirror by using a Neumann condition between regions I and II (through continuity of the $\vec{B}$ field).

This mode function can now be used to calculate the density of fluctuations around the focal point, to obtain the change in excited level shifts and spontaneous emission rates, and to find the ground-state Casimir-Polder shifts as a function of the mirror's numerical aperture.

V. QED EFFECTS CLOSE TO THE FOCUS OF A SPHERICAL MIRROR

We can now calculate the QED effects on the atomic electron from Eqs. (4), (5), and (54). The modified decay and level shifts are given by

$$\gamma(\vec{r}) = \frac{2d^2\omega_0\Lambda}{\hbar c}|\phi_{\vec{k}_0}(\vec{r})|^2 \tag{55}$$

and

$$\Delta_{e,g}(\vec{r}) = \frac{2d^2\Lambda\omega_0^2}{\hbar c}\int\frac{dk}{k}|\phi_{\vec{k}}(\vec{r})|^2\mathrm{P}\left(\frac{1}{k\pm k_0}\right), \tag{56}$$

where

$$|\phi_{\vec{k}}(\vec{r})|^2 = \frac{k^2}{\Lambda}\int_{2\pi}\frac{d\vec{\Omega}}{4\pi}\{1-\rho(\vec{\Omega})\cos[2(kR+\vec{k}\cdot\vec{r})]\}. \tag{57}$$

The dependence of the function ϕ on the b modes is now explicitly given by $\vec{k}$. In the last equation, we use the fact that the spherical harmonics form an orthonormal set of modes. We also introduce $\rho = 1-T$, the reflectivity of the mirror.

We can now also include polarization and get

$$\begin{aligned}|\phi_{\vec{k}}(\vec{r})|^2 = \frac{k^2}{\Lambda}\int_{2\pi}\frac{d\vec{\Omega}}{4\pi}\frac{3}{2}&\left(1-\left|\frac{\vec{d}\cdot\vec{\Omega}}{d}\right|^2\right)\\ &\times\{1-\rho\cos[2(kR+\vec{k}\cdot\vec{r})]\}.\end{aligned} \tag{58}$$

If we set ρ to zero everywhere, we recover the density of vacuum fluctuations in free space.

A. Real photon processes

The spontaneous decay, normalized to the free-space decay rate γ_{FS}, is

$$\begin{aligned}\overline{\gamma}(\vec{r}) = \frac{3}{2}\int_{2\pi}\frac{d\vec{\Omega}}{4\pi}&\left(1-\left|\frac{\vec{d}\cdot\vec{\Omega}}{d}\right|^2\right)\\ &\times\{1-\rho\cos[2(k_0R+\vec{k}_0\cdot\vec{r})]\}.\end{aligned} \tag{59}$$

This quantity is plotted in Fig. 2 as a function of the numerical aperture [defined as NA$=\sin(\alpha)$], for a linearly polarized dipole positioned at $\vec{r}=\vec{0}$, and orthogonal to the mirror axis. Spontaneous emission is found to vanish for a mirror position such that $\cos(2k_0R)=0$, i.e., at the node. A twofold increase in the spontaneous emission rate is found when $\cos(2k_0R)=1$, at the antinode. We note that for the numerical aperture used in Ref. [12] (NA $=0.4$, i.e., 4% of solid angle), a spontaneous emission rate change of 24% is predicted. Such a, perhaps unexpectedly, large change of a decay rate may be understood by noting that the factor of 2 due to the interference between the reflected and direct amplitudes translates into a factor of 4 in density (for "small" numerical apertures). Together with the inclusion of the polarization properties of the dipole emission, another factor of $3/2$ is gained, which in total gives $(3/2\times 4)\times 0.04 = 0.24$. The difference between the observed 1% change of the excited-state population in Ref. [12] and the 24% modification of the spontaneous emission predicted here can be partly explained by residual atomic motion, finite spatial overlap, finite temporal coherence, or multilevel effects in the experiment.

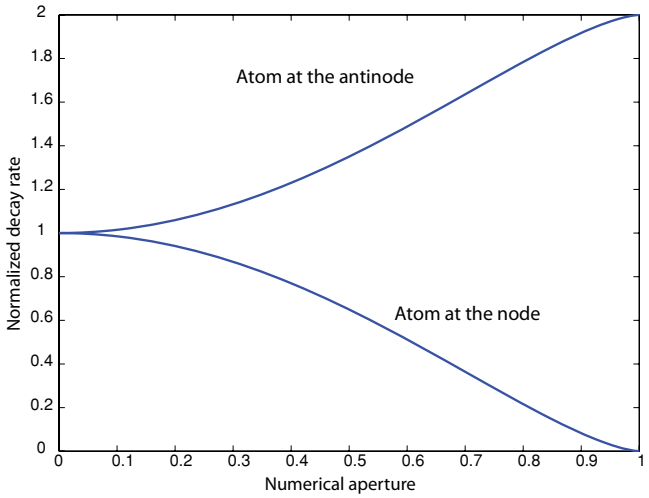

FIG. 2. (Color online) Spontaneous decay rate as a function of the spherical mirror numerical aperture for an atom at the mirror focus. Top curve: The atom is at the antinode of the standing wave formed by its retroreflected field. Bottom curve: The atom is at the node of the standing wave. Large changes in the spontaneous emission rate are already expected for moderate numerical apertures.

We can compute the modification of the decay rate as a function of distance from the focus to estimate the sensitivity to mirror, or lens, positioning. Figure 3 shows the dependence of γ for an atom that is displaced away from the focus of a hemispherical mirror and where the mirror is positioned such that $|\phi_{\vec{k}}(\vec{r}=\vec{0})|^2 = 0$. The spontaneous emission rate is close to zero within a volume λ^3 around the focus and oscillates for a few wavelengths until it reaches the free-space value. More precise formulas must be used, however, when the atom is far from the focus, as the approximation $kR \gg l(l+1)$ is no longer valid for large distances from the focus [40].

The excited-state level shift will also be altered in the same way because of a modified coupling to the retroreflected

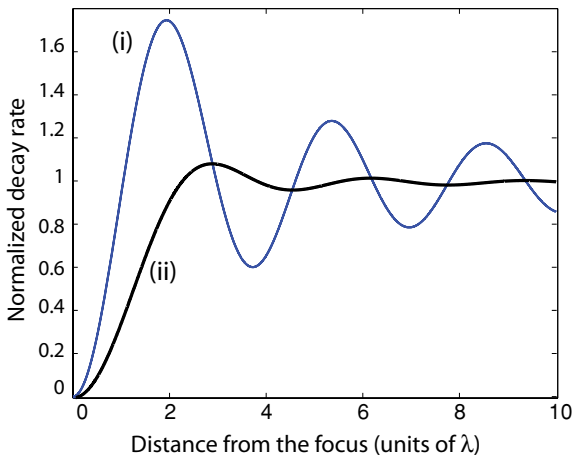

FIG. 3. (Color online) Spontaneous decay rate of an atom as it is displaced from the focus, in the case of a full-hemispherical mirror. Here the mirror is positioned such that a node of the standing wave is at the focus. Trace (i) corresponds to a scenario where the atom is displaced along the mirror axis. Trace (ii) is when the atom is displaced perpendicular to the mirror axis.

modes. We find after contour integration that the excited-state shift, normalized to the free-space decay rate, is

$$\overline{\Delta}_e(\vec{r}) = \frac{3}{2}\sum_b |\phi_b(\vec{r})|^2 \mathrm{P}\left(\frac{1}{\omega_b-\omega_0}\right) = \frac{3}{2}\int_{2\pi}\frac{d\vec{\Omega}}{4\pi}\left(1-\left|\frac{\vec{d}\cdot\vec{\Omega}}{d}\right|^2\right)\rho\sin[2(k_0R+\vec{k}_0\cdot\vec{r})]. \tag{60}$$

This gives an oscillatory level shift of amplitude ρ at the focus. For a full half mirror, the level shift completely cancels for mirror positions such that $k_0R = n\pi$, where the decay rate is also zero. Its evolution with numerical aperture is similar to the spontaneous emission rate change. Such large level shift variations can yield a strong confining potential and would be interesting to study experimentally with large-numerical apertures, similarly to what is done in Ref. [48].

B. Virtual photon processes

The Lamb shift of the ground state can be computed in the same way as the excited-state shift. In the simple case of a full half mirror, and with the atom at the mirror focus, we get

$$\Delta_g(0) = \frac{\gamma_{\mathrm{FS}}}{k_0}\int_0^{mc/\hbar} dk\,\frac{k}{k_0+k}\sin^2(kR). \tag{61}$$

We can write this result as a sum of three terms that can be easily integrated: the electron self-energy, the free-space Lamb shift, and the Casimir-Polder shift. The electron self-energy is

$$\Delta_g^{\mathrm{SE}} = \gamma_{\mathrm{FS}}\frac{K}{2k_0}\left[1+\frac{\sin(2KR)}{2KR}\right], \tag{62}$$

where we write $K = mc/\hbar$. This quantity is identified by setting k_0 to zero in Eq. (61) and in fact cancels with the shift from the $\hat{A}^2$ part of the Hamiltonian, as can be easily checked. This procedure is known as mass renormalization [30]. The free-space Lamb shift is

$$\Delta_g^{\mathrm{FS}} = \gamma_{\mathrm{FS}}\ln\left(\frac{k_0}{K+k_0}\right). \tag{63}$$

The modified Lamb shift (or Casimir-Polder shift), the only observable quantity, is

$$\Delta_g^{\mathrm{CP}} = \gamma_{\mathrm{FS}}\int_{2KR}^{2k_0R}\frac{dx}{x}\cos(x-2k_0R). \tag{64}$$

The Casimir-Polder shift goes to zero for very large mirror-atom distances ($2k_0R \gg 1$) as expected and can be approximated by

$$\Delta_g^{\mathrm{CP}} = \frac{\gamma_{\mathrm{FS}}}{(k_0R)^2}, \tag{65}$$

closer to the mirror (but always at the focus). We note that Δ_g^{CP} drops more slowly with distance than in the plane mirror case, where it decreases as $\gamma_{\mathrm{FS}}/(k_0R)^4$ [27]. The difference lies in the fact that there the mirror does not cancel as many electromagnetic modes, which yields a faster decay of the QED effects with distance.

As an example, using a decay rate of 15 MHz, a wavelength of 493 nm (the $S_{1/2}$ to $P_{1/2}$ transition of $^{138}Ba^+$), and a mirror distance of 1 cm gives a Lamb shift of 100 Hz, which is

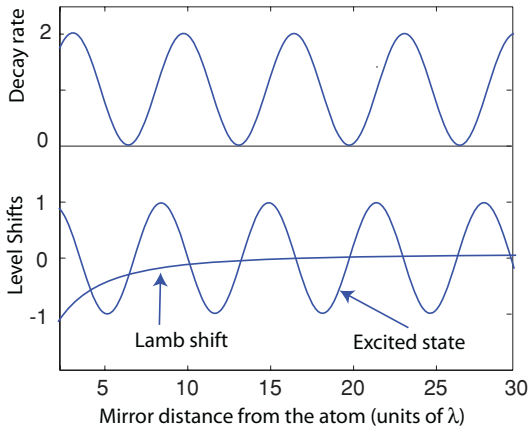

FIG. 4. (Color online) Normalized spontaneous decay rate and excited- and ground-state shifts of an atom as a function of the mirror-atom distance, in the case of a full-hemispherical mirror. Atom at the mirror focus.

experimentally measurable using modern spectroscopic tools [49]. The complete level structure will have to be used for a precise estimation of the total shift [32,43], but this result is encouraging for experimental investigations of Casimir-Polder shifts using trapped atoms.

The force on a trapped atom associated to the Casimir-Polder shift may be computed easily from this formula [40]. It would also be interesting to study how Casimir photons created by an oscillating mirror [50], as well as real photons "modulated" by the mirror [51], affect the center-of-mass motion of a trapped atom with a high-numerical-aperture mirror.

To summarize these results, the modified decay and both ground and excited level shifts are plotted in Fig. 4 for a full hemispherical mirror. The decay rate shows undamped oscillations between full suppression and maximum enhancement as a function of mirror distance (or mirror radius of curvature). The excited-state level shift oscillates between $-\gamma_{\rm FS}$ and $\gamma_{\rm FS}$, whereas the ground-state shift damps out as a function of mirror distance.

VI. CONCLUSION

In conclusion, we have demonstrated that a single spherical mirror reflecting only half of the emitted field of a single atomic electron can be used to completely suppress the atom's spontaneous emission and excited level shift. We first presented a one-dimensional treatment that explained the underlying physics behind the full-spherical mirror scenario. The modification of QED atomic properties was then calculated as a function of the spherical mirror's numerical aperture beyond the paraxial approximation. Large effects were found for moderate numerical apertures and with mirror-atom distances of several wavelengths when the atom is located at the mirror focus.

This result is also relevant for the growing field of free-space coupling to single absorbers, where full absorption of a single photon field requires a large coverage of the spatial dipole emission with the incoming spatial mode. The single hemispherical mirror system may serve here as an efficient quantum memory that can release a stored excitation on demand on a two-level atom transition by controlling the mirror position in a dynamical fashion. As an application of our calculations, one also expects full super- or subradiance with two atoms interacting via large lenses covering only half of their respective dipole emission profiles; see, for example, Refs. [33,45] for studies of this effect. Last, atom trapping using the dipole force can be very efficient here, because of the steep spatial dependence of the level shift across the atom.

Finally, we calculated the Lamb shift and showed a favorable scaling of the spherical geometry over the plane mirror case. The Lamb shift scales as $\gamma_{\rm FS}/(k_0R)^2$, where R is the mirror radius of curvature. This contrasts with the $\gamma_{\rm FS}/(k_0R)^4$ scaling law found for a plane mirror. Using Rydberg atoms and high-numerical-aperture elements can potentially yield very large shifts even for atom-mirror distances of a few centimeters and serve as a precise test bed for investigations of QED.

ACKNOWLEDGMENTS

We would like to acknowledge useful discussions with C. W. Gardiner, H. Ritsch, H. Zoubi, S. Gerber, A. Daley, and P. Zoller. This work has been partially supported by the Austrian Science Fund FWF (SFB FoQuS), by the European Union (ERC advanced grant CRYTERION), and by the Institut für Quanteninformation GmbH. G.H. acknowledges support by the Marie Curie Intra-European Foundation of the European Union.

APPENDIX

We can decompose the field in region I into radial and longitudinal parts using the relation

$$\frac{1}{k}\vec{\nabla}\times[g_l(r)\vec{X}_{l,m}]=\frac{1}{kr}\frac{\partial}{\partial r}[rg_l(r)]\vec{n}\times\vec{X}_{l,m}\\ i\frac{\sqrt{l(l+1)}}{kr}g_l(kr)Y_{l,m}\vec{n}, \quad \text{(A1)}$$

where $\vec{n}=\vec{r}/|\vec{r}|$. Using the decomposition (A1), and the eigenvalues of the angular momentum operator $\vec{L}$, we then get an expression of the electric and magnetic field in spherical coordinates.

The electric field multipoles along ϕ read

$$e^{\phi}_{\rm TM}(\vec{r})=-ig_l(r)\frac{\partial}{\partial\theta}\frac{Y_{l,m}}{\sqrt{l(l+1)}}, \quad \text{(A2)}$$

$$e^{\phi}_{\rm TE}(\vec{r})=\frac{im}{kr\sin\theta}\frac{\partial}{\partial r}[rf_l(r)]\frac{Y_{l,m}}{\sqrt{l(l+1)}}. \quad \text{(A3)}$$

Along θ, we have

$$e^{\theta}_{\rm TM}(\vec{r})=\frac{-m}{\sin\theta}g_l(r)\frac{Y_{l,m}}{\sqrt{l(l+1)}}, \quad \text{(A4)}$$

$$e^{\theta}_{\rm TE}(\vec{r})=\frac{1}{kr}\frac{\partial}{\partial r}[rf_l(r)]\frac{\partial}{\partial\theta}\frac{Y_{l,m}}{\sqrt{l(l+1)}}, \quad \text{(A5)}$$

and along r,

$$e^{\rm r}_{\rm TE}(\vec{r})=-i\frac{\sqrt{l(l+1)}}{kr}f_l(r)Y_{l,m}. \quad \text{(A6)}$$

[1] E. M. Purcell, Phys. Rev. **69**, 681 (1946).
[2] M. Brune, P. Nussenzveig, F. Schmidt-Kaler, F. Bernardot, A. Maali, J. M. Raimond, and S. Haroche, Phys. Rev. Lett. **72**, 3339 (1994).
[3] D. J. Heinzen and M. S. Feld, Phys. Rev. Lett. **59**, 2623 (1987).
[4] P. W. H. Pinkse, T. Fischer, P. Maunz, and G. Rempe, Nature (London) **404**, 365 (1994).
[5] A. Kreuter, C. Becher, G. P. T. Lancaster, A. B. Mundt, C. Russo, H. Haffner, C. Roos, J. Eschner, F. Schmidt-Kaler, and R. Blatt, Phys. Rev. Lett. **92**, 203002 (2004).
[6] C. J. Hood, T. Lynn, A. Doherty, A. Parkins, and H. Kimble, Science **287**, 1447 (2000).
[7] C. I. Sukenik, M. G. Boshier, D. Cho, V. Sandoghdar, and E. A. Hinds, Phys. Rev. Lett. **70**, 560 (1993).
[8] R. H. Dicke, Phys. Rev. **93**, 99 (1954).
[9] R. G. DeVoe and R. G. Brewer, Phys. Rev. Lett. **76**, 2049 (1996).
[10] T. Wilk, A. Gaetan, C. Evellin, J. Wolters, Y. Miroshnychenko, P. Grangier, and A. Browaeys, Phys. Rev. Lett. **104**, 010502 (2010).
[11] L. Isenhower, E. Urban, X. L. Zhang, A. T. Gill, T. Henage, T. A. Johnson, T. G. Walker, and M. Saffman, Phys. Rev. Lett. **104**, 010503 (2010).
[12] J. Eschner, C. Raab, F. Schmidt-Kaler, and R. Blatt, Nature (London) **413**, 495 (2001).
[13] M. A. Wilson, P. Bushev, J. Eschner, F. Schmidt-Kaler, C. Becher, R. Blatt, and U. Dorner, Phys. Rev. Lett. **91**, 213602 (2003).
[14] U. Dorner and P. Zoller, Phys. Rev. A **66**, 023816 (2002).
[15] N. Lindlein *et al.*, Laser Phys. **17**, 927 (2007).
[16] M. Stobinska, G. Alber, and G. Leuchs, Europhys. Lett. **86**, 14007 (2009).
[17] G. Zumofen, N. M. Mojarad, V. Sandoghdar, and M. Agio, Phys. Rev. Lett. **101**, 180404 (2008).
[18] I. Gerhardt, G. Wrigge, P. Bushev, G. Zumofen, M. Agio, R. Pfab, and V. Sandoghdar, Phys. Rev. Lett. **98**, 033601 (2007).
[19] G. Wrigge, I. Gerhardt, J. Hwang, G. Zumofen, and V. Sandoghdar, Nature Phys. **4**, 60 (2008).
[20] M. K. Tey, Z. Chen, S. A. Aljunid, B. Chng, F. Huber, G. Maslennikov, and C. Kurtsiefer, Nature Phys. **4**, 924 (2008).
[21] L. Slodička, G. Hétet, S. Gerber, M. Hennrich, and R. Blatt, Phys. Rev. Lett. **105**, 153604 (2010).
[22] A. N. Vamivakas *et al.*, Nano Lett. **7**, 2892 (2007).
[23] J. N. Munday, F. Capasso, and V. Adrian Parsegian, Nature (London) **457**, 170 (2009).
[24] S. Zaheer, S. J. Rahi, T. Emig, and R. L. Jaffe, Phys. Rev. A **81**, 030502 (2010).
[25] O. Kenneth and I. Klich, Phys. Rev. Lett. **97**, 160401 (2006).
[26] R. B. Rodrigues, P. A. M. Neto, A. Lambrecht, and S. Reynaud, Phys. Rev. Lett. **96**, 100402 (2006).
[27] H. B. G. Casimir and D. Polder, Phys. Rev. **73**, 360 (1948).
[28] R. Blatt and D. Wineland, Nature (London) **453**, 1008 (2008).
[29] Y. R. P. Sortais *et al.*, Phys. Rev. A **75**, 013406 (2007).
[30] P. W. Milonni, *The Quantum Vacuum: An Introduction to Quantum Electrodynamics* (Academic, San Diego, 1994).
[31] K. Kakazu and Y. S. Kim, Phys. Rev. A **50**, 1830 (1994).
[32] G. Barton, J. Phys. B **7**, 2134 (1974).
[33] J. Kastel and M. Fleischhauer, Phys. Rev. A **71**, 011804(R) (2005).
[34] H. Chew, J. Chem. Phys. **87**, 1355 (1987).
[35] T. Boyer, Phys. Rev. **174**, 1764 (1968).
[36] V. V. Klimov, V. S. Letokhov, and M. Ducloy, Phys. Rev. A **56**, 2308 (1997).
[37] C. R. Hagen, Phys. Rev. D **61**, 065005 (2000).
[38] K. A. Milton, Phys. Rev. D **55**, 4940 (1997).
[39] M. Stobińska and R. Alicki, e-print arXiv:0905.4014v1 [quant-ph].
[40] J. M. Daul and P. Grangier, Eur. Phys. J. D **32**, 181 (2005).
[41] J. Dalibard, J. Dupont-Roc, and C. Cohen-Tannoudji, J. Phys. **43**, 1617 (1982).
[42] D. Meschede, W. Jhe, and E. A. Hinds, Phys. Rev. A **41**, 1587 (1990).
[43] E. A. Hinds and V. Sandoghdar, Phys. Rev. A **43**, 398 (1991).
[44] F. Dubin, D. Rotter, M. Mukherjee, C. Russo, J. Eschner, and R. Blatt, Phys. Rev. Lett. **98**, 183003 (2007).
[45] S. Rist, J. Eschner, M. Hennrich, and G. Morigi, Phys. Rev. A **78**, 013808 (2008).
[46] J. D. Jackson, *Classical Electrodynamics*, 2nd ed. (Wiley, New York, 1975).
[47] W. D. Collins, Arch. Ration. Mech. Anal. **10**, 249 (1962).
[48] P. Bushev, A. Wilson, J. Eschner, C. Raab, F. Schmidt-Kaler, C. Becher, and R. Blatt, Phys. Rev. Lett. **92**, 223602 (2004).
[49] C. F. Roos, M. Chwalla, K. Kim, M. Riebe, and R. Blatt, Nature (London) **443**, 316 (2006).
[50] L. Rizzuto, Phys. Rev. A **76**, 062114 (2007).
[51] A. Glaetzle, K. Hammerer, A. Daley, R. Blatt, and P. Zoller, Opt. Commun. **283**, 758 (2010).